19th International Conference on
Adaptive Structures and Technologies
October 6-9, 2008
Ascona, Switzerland

Multistable Tape-Spring Assemblies for Morphing Aerofoil Applications

S. Daynes[1]*, K. D. Potter[2], P. M. Weaver[3]
[1] PhD Student, Department of Aerospace Engineering, University of Bristol, UK.
[2] Reader, Department of Aerospace Engineering, University of Bristol, UK.
[3] Reader, Department of Aerospace Engineering, University of Bristol, UK.

* Bristol. BS8 1TR. Tel.: + 44 117 92 87704. Fax: + 44 117 927 2771. E-mail: stephen.daynes@bristol.ac.uk

ABSTRACT

Changing the aerodynamic forces acting on an aerofoil is most commonly done by camber change using an actuated pin-jointed control surface at the trailing edge. There can be significant mass penalties with such devices and achieving a smooth camber variation is difficult. This work presents a design for an aerofoil section which has at least two stable camber geometries. The aerofoil's multistability derives from the use of a novel tape-spring assembly. A tape-spring is effectively a cylindrical shell. They possess the unusual mechanical property of being able to be folded elastically and lock when straightened. The design case considered is based on a typical helicopter main rotor blade. The multistable device is used to improve the performance of the rotor blade during the transition between hover and forward flight. Force-displacement characteristics of the flap are found experimentally and compared with finite element and analytical models. Both modelling techniques are in good agreement with the manufactured demonstrator.

Keywords: Morphing aircraft, Multistable structures, Residual stress, Nonlinear deformations.

1. INTRODUCTION

The most common technique to change the aerodynamic forces acting on an aerofoil is to perform a camber change. The conventional way of achieving this movement is with a pin-jointed control surface (i.e. a flap/rudder/aileron) at the trailing edge with a corresponding actuator system. Such solutions require mechanical joints, bearings, movable parts, etc. There can be a significant mass penalty with such components even if the actual structure is optimised for mass. In addition, using a limited number of finite joints greatly limits the possibility of achieving a smooth camber variation. This work presents a design for an aerofoil section which has at least two stable camber geometries. The design's multistability derives from the use of thin-walled strips of material with a curved cross-section known as tape-springs [1].

There has been significant effort in the space industry in recent years to develop deployable structures with low cost, simple, self-locking hinges. This paper presents a design for a novel self locking hinge which has more than one stable configuration. This is achieved by using two sets of tape-springs to provide two distinct locking moments. Several monostable tape-spring hinge designs have already been investigated, see Figure 1 [2-5]. From these studies several benefits over conventional hinge mechanisms have emerged:

- No friction and backlash.

- Elastic locking (highly repeatable and accurate).
- No moving parts.
- Easily tailored mechanical properties.
- Simple to manufacture.
- Low cost.
- Light weight.

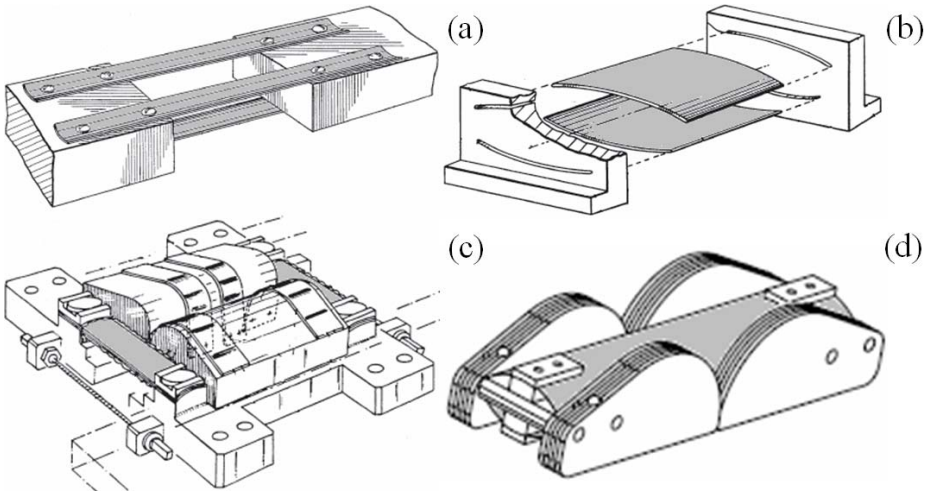

Figure 1. Tape-spring hinge designs (a) Vyvyan, (b) Chiappetta et al., (c) Auternaud et al., (d) Watt and Pellegrino.

The design of multistable structures requires an understanding of several different disciplines and their various interactions. Lightweight design is an extremely important consideration in the aerospace industry with the aim of creating structures with a high strength-to-weight ratio. However, for adaptive structures deformability is also a key consideration which can often be in conflict with the requirement for a lightweight design. Conventional mechanisms, such as flaps, are highly shape adaptable and can carry high loads but cannot be called lightweight. Compliant mechanisms offer the advantage of being both shape adaptable and lightweight. At present, however, the load carrying capability of compliant mechanisms tends to be relatively poor [6].

The Intelligent Responsive Composite Structures (IRCS) program at the University of Bristol aims to identify methods by which localised segments of an aerofoil section may be shape adapted for performance and other advantages. The total IRCS system comprises of multistable constructions that change shape when forced by actuators. The design case here is based on a typical modestly cambered helicopter main rotor blade section with a 100mm long flap. The purpose of the IRCS device is to improve the performance of the rotor blade in both the hover and forward flight regimes by having more than one stable shape. It is required that the camber change required is approximately 0^o to $+10^o$ trailing edge deflection upon command. A positive deflection is defined as vertically downwards from the trailing edge. The rotor then remains in a constant state until actuated by the pilot, i.e. after transit from hover to forward flight etc. At this point the multistable structure is actuated to change shape. Changes of camber state are thus relatively infrequent and so a coarse control of the structure can be tolerated.

In this work, the manufactured multistable aerofoil flap is presented. The force-displacement characteristics of the aerofoil flap are then found experimentally. Analytical and finite element (FE) models are also presented and compared with the experimental demonstrator. Finally some areas for future research are suggested. The novelty of this current work lies in the fact that the aerofoil flap can remain in one of several stable geometries and still withstand significant external loading. A further novel feature is that, unlike a conventional flap, an actuator is only required to do work during transition between these stable geometries. It is energetically preferential for a multistable structure to take only one of its stable geometries. Therefore if it is known what state the structure is in then there is little need for a continuously monitoring position feedback control system.

2. STRUCTURAL DESIGN

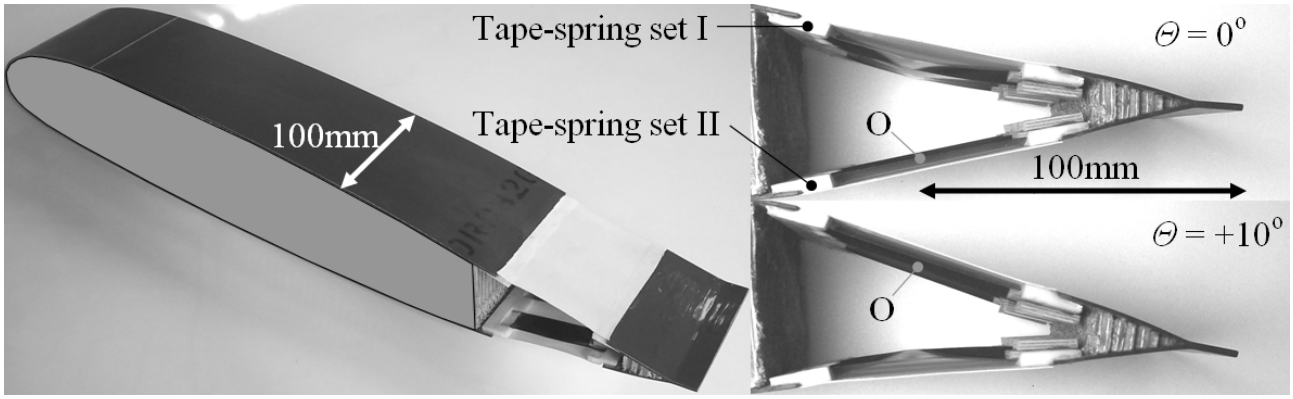

Figure 2. Aerofoil section with multistable tape-spring flap.

The aerofoil section with a multistable flap manufactured is shown in Figure 2. The multistable flap consists of two sets of tape-springs. Three tape-springs are attached to the upper side of the aerofoil (set I) and another three tape-springs are attached to the lower side (set II). The aerofoil flap shown has two stable geometries; it is stable when deflected at both 0^o and $+10^o$. When the trailing edge is in the 0^o configuration the lower surface tape-springs are straight and rigid whilst the other tape-springs are buckled. The opposite is true for the $+10^o$ configuration. This can happen because the angles that the tape-springs are clamped at are approximately 10^o out of line relative to each other. The resistance of the straight tape-springs to buckling will always be substantially larger than the restoring force created by the buckled tape-springs, hence multistability can occur. Transition between the two stable shapes may be achieved by external actuation. The tape-springs are attached to the composite skin of the aerofoil using four ABS plastic attachments. These attachments were manufactured using the layer manufacturing technique for accuracy. The two attachments connecting the main rotor blade structure to the tape-springs provide a clamped boundary condition. The other two attachments at the trailing edge allow translational movement. Rubber adaptive skins are used to cover the tape-spring hinge assembly. These skins are pretensioned during manufacture. It is shown later that this pretension can aid multistability. Unlike a conventional flap solution this design has no surface discontinuities when the flap rotates. This design feature has the potential to improve aerodynamic effects such as the point of trailing edge separation and localised pressure spikes. The absence of surface discontinuities also ensures the cambering aerofoil remains weather tight.

To quantify the structural stiffnesses and snap-through characteristics of the multistable flap the manufactured aerofoil was subject to a set of load-displacement tests. The manufactured aerofoil was mounted over the static cross-head of an INSTRON type 3343 1kN test machine, see Figure 3. The virtual hinge point ‘O’ of the multistable structure was mounted on the test machine so as to be exactly 90mm away from the line of action of the applied load. It is assumed that the pivot point will occur half way along the tape-spring set to be buckled. Compressive load was then applied to the flap using a small metal pointer so as to obtain load-displacement data. For practical purposes, the test machine’s frame and the aerofoil’s structure in front of the flap region is assumed to be rigid. From this force-displacement data and knowledge that the effective flap length is 100mm, moment-rotation data was obtained. Two compressive force-displacement tests were carried out in opposing directions. From these two tests the moment-rotation characteristics of the multistable aerofoil were derived, as presented in the Results and Discussion section.

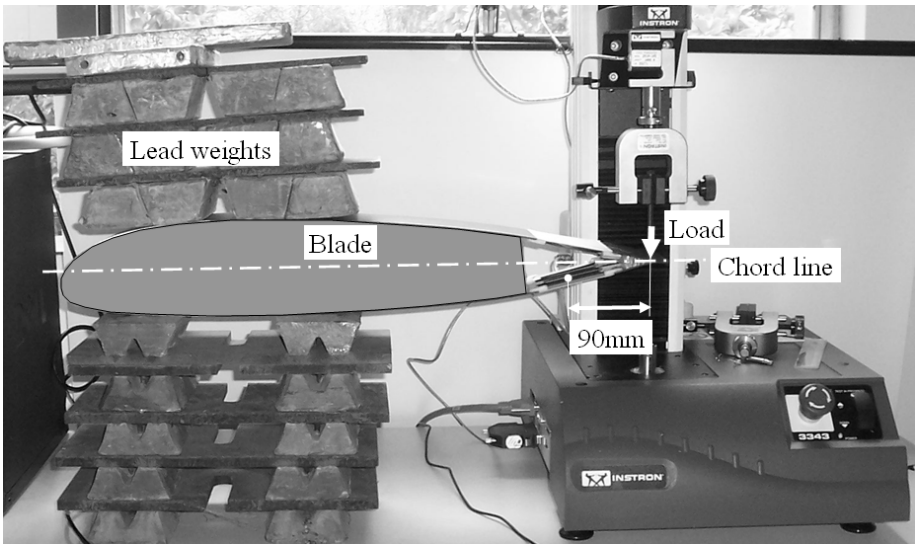

Figure 3. Multistable flap force-displacement measurement.

3. ANALYTICAL MODEL

A tape-spring is effectively a cylindrical shell with radius of curvature R, subtended angle α and thickness t. They possess the unusual mechanical property of being able to be folded elastically and lock when straightened. The particular geometric properties of the tape-spring being studied are shown in Figure 4. The tape-springs are manufactured from steel with Young's modulus, E, of 200GPa and Poisson's ratio, v, of 0.3.

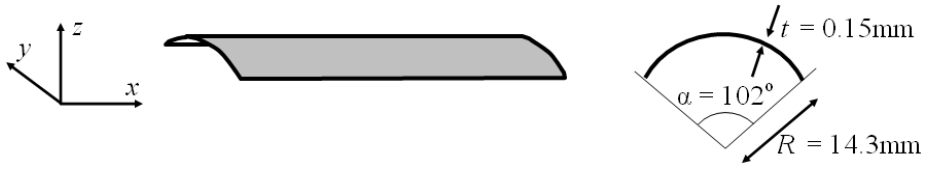

Figure 4. Tape-spring geometry.

The simplified moment-rotation characteristics of a tape-spring are shown in Figure 5 [7]. A tape is said to be subject to *opposite-sense bending* if the longitudinal and transverse curvatures are in the opposite sense. If these curvatures are in the same sense then the tape is subject to *equal-sense bending*. For opposite-sense bending the moment-curvature relationship is effectively linear up to the *snap-through* moment M_{+}^{max}. Up to this critical moment a tape-spring possesses a high stiffness. After this snap-through point the moment reduces quickly to a constant value of M_{+}^{*} due to the formation of an elastic fold. For equal-sense bending the tape-spring is much less stiff and snap-through occurs at a much lower bending moment M_{-}^{*}.

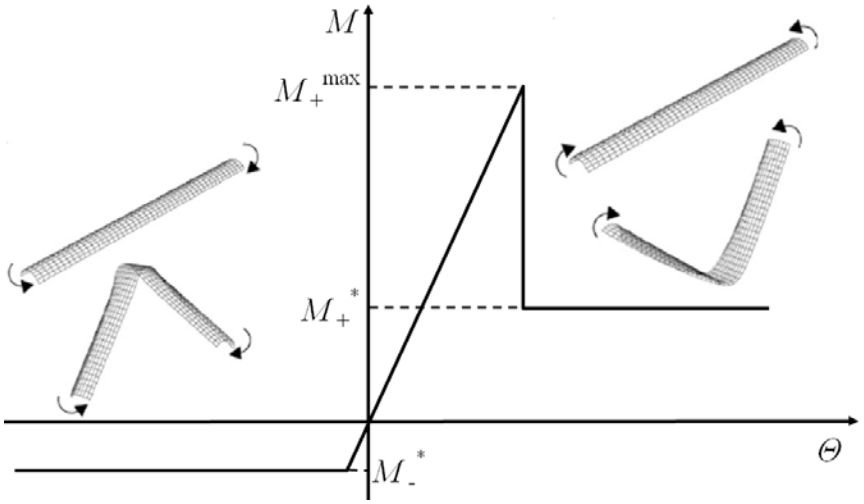

Figure 5. Schematic tape-spring moment-rotation diagram.

Wuest was the first to obtain expressions for the moment-curvature relationship for an isotropic tape-spring of infinite length [8]. By integrating the moments about the transverse axis for the whole cross-section of the tape-spring the end moment can be obtained. The snap-through moment $M_+^{\max}$ is obtained by maximising Equation (1).

$$M = \int_{-s/2}^{s/2} (M' - N'w)dy = sD\left(\kappa_l + \frac{v}{R} - v\left(\frac{1}{R} + v\kappa_l\right)F_1 + \frac{1}{\kappa_l}\left(\frac{1}{R} + v\kappa_l\right)^2 F_2 \right) \tag{1}$$

where $s=2R\sin(\alpha/2)$ is the width of the tape-spring, w is the out-of-plane deflection and κ_l is the longitudinal curvature. M' and N' are the bending moment per unit length and axial force per unit length respectively. The bending stiffness is defined as $D = Et^3/12(1-v^2)$. The terms F_1 and F_2 are defined as

$$\begin{aligned} F_1 &= \frac{2}{\lambda}\frac{\cosh\lambda - \cos\lambda}{\sinh\lambda + \sin\lambda} \\ F_2 &= \frac{F_1}{4} - \frac{\sinh\lambda\sin\lambda}{(\sinh\lambda + \sin\lambda)^2} \end{aligned} \tag{2}$$

where $\lambda = \sqrt[4]{3(1-v^2)}s \Big/ \sqrt{t/\kappa_l}$. Wuest also observed that the longitudinal curvature κ_l in the fold region is equal to the undeformed transverse curvature $\kappa_t=1/R$. The corresponding bending moment M^* in a fold region after snap-through is given by [9]

$$M^* = DR\alpha(\kappa_l + v\kappa_t) \tag{3}$$

For opposite-sense bending $\kappa_t=1/R$ and $\kappa_l=1/R$. For equal-sense bending again $\kappa_t=1/R$ but $\kappa_l=-1/R$. Substituting these values into Equation (3) yields expressions for the steady moments M_+^* and M_-^* respectively.

$$\begin{aligned} M_+^* &= D\alpha(1+v) \\ M_-^* &= -D\alpha(1-v) \end{aligned} \tag{4}$$

As previously mentioned the required moment to buckle the opposite-sensed tape-springs $M_+^{\max}$ will always be greater than the internal moment of the folded tape-springs M_+^*. The forces and

moments exerted on the multistable flap are shown in Figure 6. The contribution of the skin to aid multistability in this design is also very important and should not be overlooked. For example, when $\Theta = 0^o$ the upper skin is exerting a force of $k_I(a_I\text{-}a_{I0})$ with a moment arm of length b_I=37mm from the virtual pivot point. Here k_I refers to the stiffness of the upper skin, a_I is the upper skin's length and a_{I0} is the skin's length prior to pre-stretch during manufacture. In the Θ=0^o configuration the lower skin exerts an elastic force of $k_{II}(a_{II}\text{-}a_{II0})$. However, its corresponding bending moment is negligible because its moment arm b_{II} is very small. In the $\Theta = 10^o$ configuration the virtual pivot point of the structure switches to the upper set of tape-springs making distance b_{II} much larger at 37mm and b_I is instead very small. Here $a_{I0} = a_{II0} = 55$mm and $k_I = k_{II} = 1.73$N/mm. Assuming the tape-spring assembly behaves like a one degree-of-freedom mechanism the required snap-through moment $M_{snap}(\Theta)$ to actuate the structure between its two stable configurations can therefore be expressed as:

$$M_{\text{snap}}(\Theta) = M_{\text{II}}(\Theta) - M_{\text{I}}(\Theta) + k_{\text{I}}b_{\text{I}}(a_{\text{I}} - a_{\text{I0}}) - k_{\text{II}}b_{\text{II}}(a_{\text{II}} - a_{\text{II0}}) \tag{5}$$

where $M_I(\Theta)$ and $M_{II}(\Theta)$ are the reaction moments from tape-spring sets I and II respectively. When $\Theta = 0^o$ then $M_I(\Theta)=M_+^*$. Likewise when Θ=10^o then $M_{II}(\Theta)=M_+^*$. For simplicity the analytical model shall assume that one set of tape-springs is always buckled and exerting the moment M_+^* during transition between the two stable geometries.

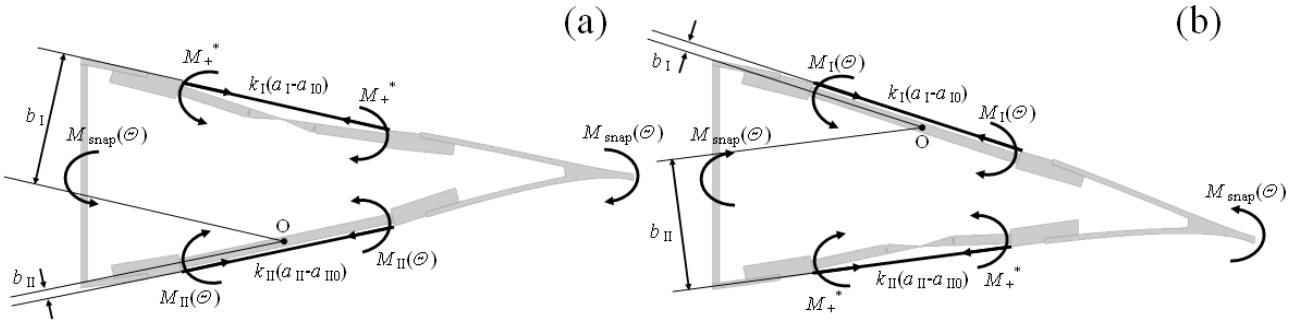

Figure 6. Forces and moments diagrams for tape-spring assembly when (a) Θ=0^o and (b) Θ=10^o.

4. FINITE ELEMENT MODELLING

A FE model of the multistable assembly was created using ABAQUS [10], and is shown in Figure 7. Only one set of half tape-springs were modelled with a symmetric boundary condition applied along the centre line of the tape-springs in the fixed global 1-axis. The FE model was meshed using 9×50 4-node doubly curved general purpose shell elements (S4R). A logarithmic bias of 2 was applied to the 50 nodes in the *x*-direction so a finer mesh was generated towards the centre since this is the region where snap-through occurs. Convergence studies on the mesh size were carried out in order to determine the accuracy of the model and good results were obtained for this particular mesh. The length of the tape-springs modelled was 65mm and they are positioned relative to each other to match the geometry of the manufactured demonstrator model. The two tape-spring ends attached to the main rotor blade structure have fully clamped boundary conditions assigned to them. Two multi point constraints (MPCs) are applied to the other two tape-spring ends to prevent cross-section distortions. The two MPC reference nodes were coupled together using the 'slot' and 'revolute' connector sections, as defined in the ABAQUS 6.6-1 user guide. This connector enables the sliding boundary conditions at the trailing edge to be modelled. Bending moments are applied to these MPC reference nodes to represent the bending moments caused by the two skins. The bending moments for skins I and II are estimated as $k_I(a_I\text{-}a_{I0})b_I$ and $k_{II}(a_{II}\text{-}a_{II0})b_{II}$ respectively. Here a_I and a_{II} are taken to be 70mm because this is the experimentally observed maximum skin length prior to snap-through occurring. The model is restricted in rotation about the global 3-axis to $10^o \leq \Theta \leq 0^o$ so equal-sense

bending of the tape-springs cannot occur.

The snap-through analysis of the structure is achieved in several steps using geometrically non-linear "Static General" analysis simulations. At first the "Static Riks" analysis procedure was chosen so the unstable parts of the analysis could be included but convergence could not be achieved. Initially, both tape-springs are straight so the first step is to snap the lower tape-spring into its deformed position using displacement controlled deformations. After this the assembly is allowed to relax into its new geometry and the skin II bending moment is applied to the assembly. Snap-through from the $\Theta = 10^o$ configuration is then simulated by applying a bending moment about the 3-axis to one of the MPC reference nodes. This bending moment is then removed in a second relaxation step for the assembly to move into the $\Theta = 0^o$ configuration, the skin I bending moment is applied and the skin II bending moment is removed. An opposite snap-through moment is applied followed by a third relaxation step to return to the $\Theta=10^o$ configuration.

Because the analysis was a geometrically non-linear problem, solutions were found by breaking the analysis into increments. An approximate equilibrium configuration had to be found for each of these increments. A converged solution was obtained by controlling local instabilities by introducing artificial damping into the model. A damping factor of 1×10^{-4} was selected. It was important to keep this damping factor as low as possible because excessive damping may affect the accuracy of the solution obtained.

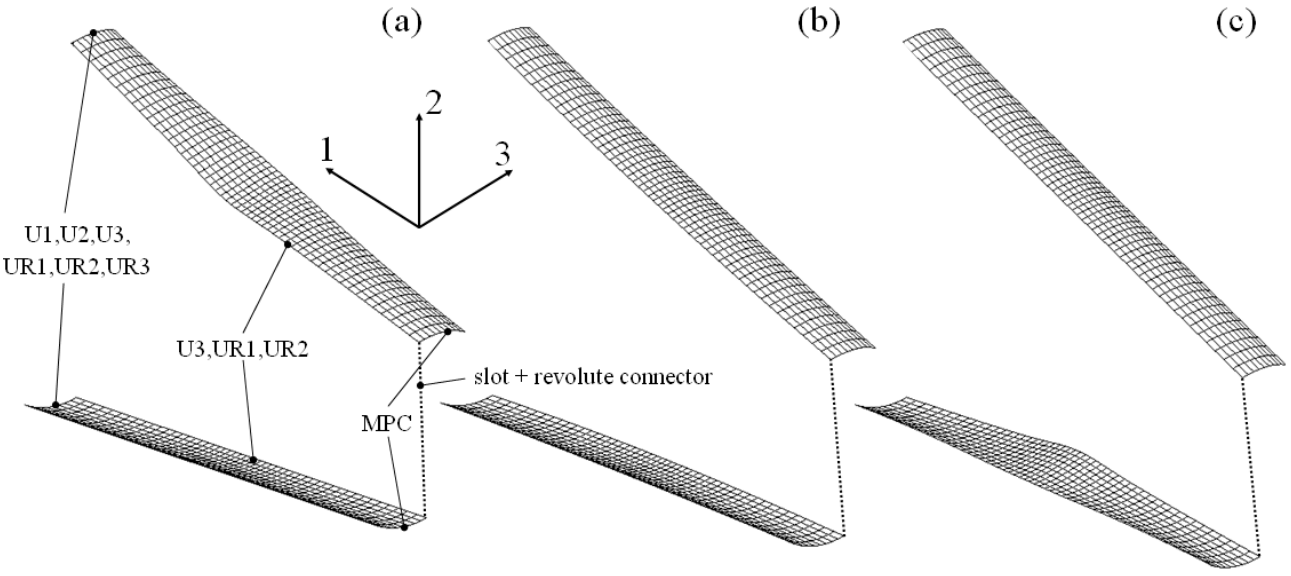

Figure 7. FE geometry with (a) $\Theta=0^o$, (b) $\Theta=5^o$ and (c) $\Theta=10^o$.

5. RESULTS AND DISCUSSION

The moment-rotation characteristics of the tape-spring assembly are shown in Figure 8. The experimental, FE and analytical results all show that for rotation to occur the applied moment must be greater than approximately ±530Nmm. This is due to the magnitude of the terms - $M_I(\Theta)+k_Ib_I(a_1-a_{I0})$ and $M_{II}(\Theta)-k_{II}b_{II}(a_{II}-a_{II0})$ in Equation (5). After this point there is a near linear moment-rotation relationship up to the point of snap-through. This near linear behaviour is modelled by the terms $M_I(\Theta)$ and $M_{II}(\Theta)$ in Equation (5). Once the snap-through moment has been applied the tape-spring assembly moves to its other stable configuration. Agreement between the FE and experimental moment-rotation results is very good. However, the FE results predict slightly higher snap-through loads; this may be because there were manufacturing imperfections in the experimental demonstrator. The FE results also predict snap-through will occur for smaller angles. The likely reason for this is due to imperfections in the experimental boundary conditions, particularly the compliance of the plastic end clamps used. The snap-through moments predicted by the analytical model are also quite

accurate although the predicted snap-through angles are substantially lower.

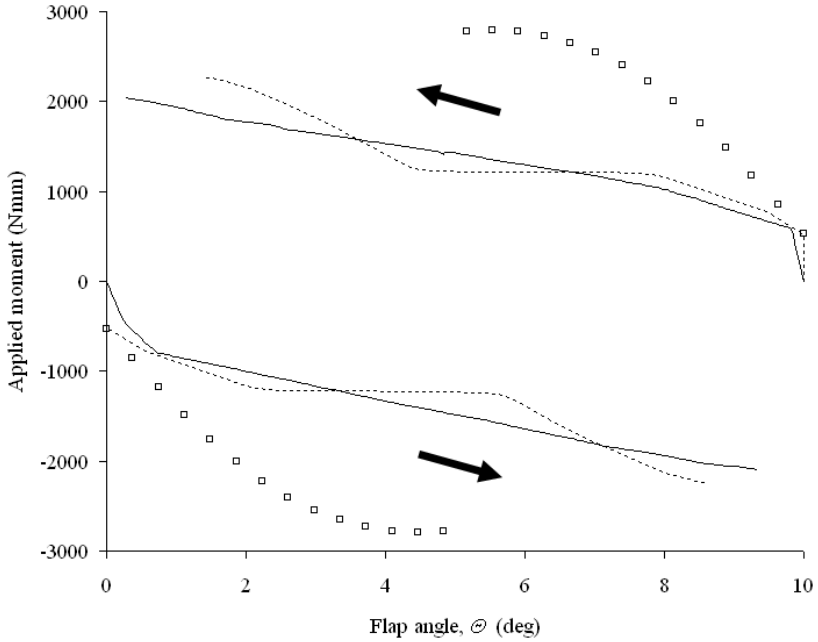

Figure 8. Moment-rotation results; — Experimental; --- FE; □ Analytical.

Figure 8 also shows that the manufactured tape-spring assembly in question is symmetrically bistable [11]. That is to say both of the structure's stable states store the same amount of strain energy. This means that the actuator will be required to do the same amount of work for transition between both stable states. An area for future research could be the study of asymmetrically bistable structures. These types of structure have unequal amounts of strain energy stored in their stable states. Asymmetric bistability could be achieved by giving the two sets of tape-springs and/or skins different mechanical properties. In reality the rotor blade will be subject to environmental loading caused by factors such as structural loads, aerodynamics, dynamics and vibrations. These may also be source of asymmetric bistability which will affect actuator performance requirements. It is also worth noting that the FE model suggests that a third stable geometry exists when Θ is approximately 5^{o}. This stable state is shown in Figure 7(b) and occurs when neither set of tape-springs are snapped-through. The existence of a third stable geometry could explain the plateaus in the FE moment-rotation results when $\Theta=5^{o}$ in Figure 8. However the force controlled "Static General" FE analysis used could not model this intermediate stable geometry. This third stable state was not observed experimentally probably because a pure bending moment was not applied to the manufactured aerofoil.

Another potential path for further investigation is the study of multistable structures with more than three stable states. Each tristable tape-spring assembly provides three stable states. Therefore, if there are n tristable assemblies then there is the potential for 3^{n} stable states. The multistable structure will approximate continuous motion as n becomes larger.

6. CONCLUSIONS

A multistable aerofoil design has been presented which can change shape between at least two different camber geometries. The trailing edge of the aerofoil is able to deflect between 0^{o} and $+10^{o}$ upon command. The aerofoil can remain in these positions without the aid of further actuation. In addition to this feature, the design solution presented is significantly lighter and simpler than a conventional pin-jointed flap. Such a multistable device could be used to improve the performance of a rotor blade during the transition between hover and forward flight. An analytical model was formulated to describe the mechanics of the multistable tape-spring assembly manufactured. The

analytical model is sufficiently accurate to estimate the snap-through moments of the structure. A FE model was also developed to model the manufacture multistable aerofoil. The FE model was able to estimate both snap-through moments and snap-through angles accurately. Future research could investigate multistable tape-spring assemblies which have more than three stable geometries and/or asymmetrically multistable structures.

REFERENCES

1. Seffen, K. A., Pellegrino, S., "Deployment dynamics of tape springs," *Proceedings of the Royal Society of London A*, Vol. 455, pp. 1003-1048 (1999).
2. Vyvyan, W. W., "Self-actuating, self-locking hinge," U.S. Patent 3386128 (June 1968).
3. Chiappetta, F. R., Frame, C. L., Johnson, K. L., "Hinge element and deployable structures including hinge element," U.S. Patent 5239793 (August 1993).
4. Auternaud, J. et al., "Self motorized antifriction joint and an articulated assembly, such as a satellite solar panel equipped with such joints," U.S. Patent 5086541 (February 1992).
5. Watt, A. M., Pellegrino, S., "Tape-Spring Rolling Hinges," *Proceedings of the 36th Aerospace Mechanisms Symposium* (May 2002).
6. Campanile, L. F., "Adaptive Structures: Engineering Applications," John Wiley & Sons Ltd., Chichester, England, Ch. 4 (May 2007).
7. Soykasap, O., "Analysis of tape spring hinges," *International Journal of Mechanical Sciences*, Vol. 49, pp. 853-860 (2007).
8. Wuest, W., "Einige anwendungen der theorie der zylinderschale," *Zeitschrift fur angewandte Mathematik und Mechanik*, Vol. 34, pp. 444-454 (1954).
9. Calladine, C. R., "Theory of Shell Structures," Cambridge University Press, Cambridge, England, (1983).
10. ABAQUS/CAE, Version 6.6-1 (2006).
11. Santer, M. J., Pellegrino, S., "Asymmetrically-Bistable Tetrahedra," *Proceedings of the 46th AIAA/ASME/ASCE/AHS/ASC Structures, Structural Dynamics and Materials Conference*, (April 2005).